Analysis of individual magnetic particle motion near a chip surface

Analysis of individual magnetic particle motion near a chip surface

Kim van Ommering,[1,2,a)] Carolien C. H. Lamers,[1,2] Jeroen H. Nieuwenhuis,[1] Leo J. van IJzendoorn,[2] and Menno W. J. Prins[1,2,b)]
[1]*Philips Research Laboratories, 5656 AE Eindhoven, The Netherlands*
[2]*Department of Applied Physics, Eindhoven University of Technology, 5600 MB Eindhoven, The Netherlands*

(Received 24 November 2008; accepted 19 March 2009; published online 21 May 2009)

We describe an analysis of the dynamics of individual superparamagnetic micro- and nanoparticles in order to quantify their magnetic properties and mobility near a chip surface. The particles are attracted to the chip surface by integrated microscopic current wires. We show that it is possible to accurately analyze particles with a diameter of about 1 μm by the magnetophoretic movement between current wires because of the very high field gradients. This reveals distinct differences in volume susceptibilities of particles with the same outer diameter. Smaller particles are characterized using the technique of confined Brownian motion analysis. By capturing 300 nm particles on a current wire with surface barriers or a focused shape, the magnetization of the particles can be measured with an accuracy better than 10%. © *2009 American Institute of Physics*.
[DOI: 10.1063/1.3118500]

I. INTRODUCTION

Magnetic micro- and nanoparticles have found their way into a large number of applications. In early applications, large ensembles of magnetic particles were used, for example, to extract biomaterial or as contrast agents in magnetic resonance imaging.[1] Presently, there is a trend to use magnetic particles in more refined ways, such as applying them as a means of transport in lab-on-a-chip devices,[2–4] as detection labels for target molecules,[5–7] or even as tools for functional biosensing in cell property research or binding force measurements.[8,9]

To improve the functioning of magnetic particles in magnetic particle-based biosensors or lab-on-a-chip devices, we have investigated several techniques to quantify the magnetic properties of individual magnetic particles. The magnetic properties are, for example, important for accurate detection in magnetic biosensors and for well-controlled transport of particles, and attached biological species, toward or over a (chip) surface.

The magnetic properties of particles are a complex function of many parameters: the type and amount of magnetic material inside the particles, the particle shape, and the internal nanostructure, such as the grain size distribution. Even within a type of particles, the particle constitution and therefore the magnetic properties can vary; therefore it is necessary to analyze particles on the single-particle level. Moreover, because there is an increasing trend in device technology toward miniaturization and integration, the particle properties need to be known under specific circumstances, such as in low magnetic fields (<10 mT) resulting from integrated electromagnetic structures.[10,11]

We present several chip designs with integrated current wires having characteristic dimensions of a particle diameter in order to analyze individual particles near a chip surface in low magnetic fields with high field gradients. Two distinct experiment types are described: magnetophoretic analysis and confined Brownian motion analysis. First, we show that it is possible to use on chip magnetophoresis to accurately analyze small particles with a diameter of about 1 μm because of the very high field gradients generated by the current wires. Next, we apply the technique of confined Brownian motion analysis to analyze the magnetic properties of particles even smaller than 1 μm.

II. MATERIALS AND METHODS

The silicon chips used in this study contain current wires with a thickness of 350 nm (10 nm molybdenum, 250 nm gold, 90 nm molybdenum) and a width between 2.4 and 3.4 μm. The wires are covered with a polished 500 nm layer of silicon nitride. Optionally the silicon nitride is covered by an 80 nm gold layer. The wire length is 150 μm. Typical currents are 20–40 mA. In this regime we observed a small temperature rise in the wire due to heat dissipation (3–13 °C). The magnetic field of the straight wire with rectangular cross-section is calculated analytically using the Biot–Savart law. The magnetic field of current wires with other shapes is calculated by simulating the current density profile using the finite element simulation program COMSOL MULTIPHYSICS® and by calculating the magnetic field from this current density profile in MATLAB® (The Mathworks, Inc.) using the Biot–Savart law.

The magnetic particles analyzed in this study are superparamagnetic beads composed of iron oxide grains in a polystyrene matrix. We analyzed three types of particles: Dynabeads® MyOne™ streptavidin C1 from Invitrogen (referred to as "Dynal 1 μm"), 1 μm superparamagnetic beads with streptavidin coating from MagSense Life Sciences, Inc. ("MagSense 1 μm"), and 300 nm Bio-Adembeads streptavidin from Ademtech ("Ademtech 300 nm"). The surfaces of

a)Electronic mail: kim.van.ommering@philips.com.
b)Electronic mail: menno.prins@philips.com.

all particles are coated with streptavidin. Scanning electron microscopy (SEM) images of the Dynal 1 μm particles showed that they are very monodisperse in size (mean size of 1.05 μm, coefficient of variation of 3%). SEM images of the MagSense particles show that they are on average larger than 1 μm and more polydisperse, with diameters ranging from 0.5 to 2.5 μm (mean size of 1.4 μm, coefficient of variation of 20%). Transmission electron microscopy (TEM) images of the Ademtech 300 nm particles show the expected mean size of 300 nm and a coefficient of variation of 30%.

The magnetic particles are used directly from the stock solution and are diluted 1000 to 20 000 times in de-ionized water. In de-ionized water the electrostatic surface charges of the particles and the chip surface are minimally shielded, which increases the mutual repulsion and suppresses sticking of the particles to the chip surface. A 10 μl drop is applied to the chip surface. The particles are observed using an optical microscope (Leica) with 160× water-immersion objective and a high-speed camera (MotionPro from RedLake, 30–250 fps). The pixel size in the movies is 62 nm. We developed particle tracking software in MATLAB based on the method of Crocker and Grier,[12] optimized for specific issues in our measurements such as a complex background, to resolve the trajectories of particles down to 150 nm in diameter with subpixel resolution (20 nm).

III. MAGNETOPHORETIC ANALYSIS

In magnetophoretic analysis, information on the magnetic properties of particles is obtained by measuring the speed of the particles induced by a magnetic field gradient. This technique was first proposed in 1960[13] and first used in a well-defined setup by Reddy *et al.*[14] in 1996. Nowadays it is the most common technique for analyzing individual particles or magnetically labeled biomaterial such as cells.[15] Usually permanent magnets or electromagnets are used to induce a known field gradient, and particles larger than a few micrometers are analyzed. For particles in the 1 μm range, field gradients are not large enough to obtain magnetically induced speeds significantly larger than the Brownian motion, which limits measurement accuracy. A variety of particles was measured by Häfeli *et al.*,[16] but for the micrometer range their error in speed determination was roughly 50%, so differences within one type of particles could not be determined accurately. Here we describe the use of integrated microscopic current wires rather than external (electro)magnets to induce well-defined and very high magnetic field gradients while staying in a low-field regime.

The speed $\mathbf{v}$ of a particle in a known magnetic field $\mathbf{B}$ with a gradient is directly proportional to the particle susceptibility χ_{par},

$$\mathbf{v} = \frac{1}{f_d}\left(\chi_{\mathrm{par}} \nabla \left(\frac{\mathbf{B}^2}{2\mu_0}\right)\right). \tag{1}$$

Here f_d is the hydrodynamic drag coefficient, which in bulk fluid is given by the Stokes drag coefficient $f_d = 6\pi\eta r$, with η the fluid viscosity and r the particle radius. The particle susceptibility χ_{par} (unit $[\mathrm{m}^3]$) is related to the volume susceptibility χ_{vol} (dimensionless) via $\chi_{\mathrm{par}} = \chi_{\mathrm{vol}} V$, with V the volume of one particle. In this equation the susceptibility of the water medium is neglected because it is much smaller than the particle susceptibility (order of 10^{-5}). The particle susceptibility includes demagnetization effects, $\chi_{\mathrm{vol}} = \chi_i/(1+N\chi_i)$, with N the demagnetization factor and χ_i the intrinsic volume susceptibility. For perfect spherical particles N is equal to 1/3. For a prolate spheroid[17] and $\chi_i = 6$, one can estimate that in order to obtain a difference of 10% in χ_{vol}, an aspect ratio of 1.2 is needed.

For the distance traveled due to the magnetic force to be negligible compared to the distance traveled by Brownian motion, the following relation should apply during the characteristic measurement time t:

$$\int \mathbf{v} dt \gg 2\sqrt{\frac{Dt}{\pi}}, \tag{2}$$

where D is the diffusion coefficient of the particles ($D = k_B T/6\pi\eta r$). For example, a 1 μm particle in water at 20 °C has a diffusion coefficient of 0.43 $\mu\mathrm{m}^2\,\mathrm{s}^{-1}$. With a typical volume susceptibility of $\chi_{\mathrm{vol}} = 2.7$ and a characteristic time of 1 s, a gradient $\nabla\mathbf{B}^2 > 0.25$ T^2/m is needed for a maximum error of 5% due to diffusion. This value is challenging for fields larger than 100 mT and even more difficult for low fields (<10 mT) but can be obtained over small distances using microscopic current wires.

A. Crossing between two wires

We designed a chip containing two parallel current wires with a width of 2.4 μm and a distance of 6 μm between the centers of the wires [see Fig. 1(a)]. With these current wires we can obtain gradients above 0.5 T^2/m over a distance of 6 μm in fields lower than 10 mT. On this chip we analyzed two types of particles: Dynal 1 μm particles and MagSense 1 μm particles. In the experiments we alternately actuated both wires to move the particles from wire to wire, and we determined the average crossing time per particle, which is directly related to the particle susceptibility [Eq. (1)]. In Fig. 1(b) the average crossing time is plotted against the diameter of the particle that is determined by measuring the apparent optical diameter in the movies and correcting this value for the diffraction.[18] We could measure crossing times with an accuracy of 3%–5%. Even though the Dynal particles are very homogeneous in size, their crossing times vary up to a factor 1.5. The crossing times of MagSense particles vary up to a factor of two, but their size also varies a factor of 1.4. All measured MagSense particles appeared to be larger than the Dynal particles probably because in a batch of mixed sizes, as is the case for MagSense particles, larger particles are attracted to the wires first.

To obtain the particle susceptibility from the crossing time using Eq. (1), two parameters need to be determined, namely, the field gradient that the particle experiences and the hydrodynamic drag coefficient. The field of the current wires is quite nonuniform; therefore we calculated the average field gradient by integrating the magnetic field energy over the particle volume using a finite element simulation in MATLAB. Because of the large variations in particle sizes in Fig. 1, this calculation was performed for each particle sepa-

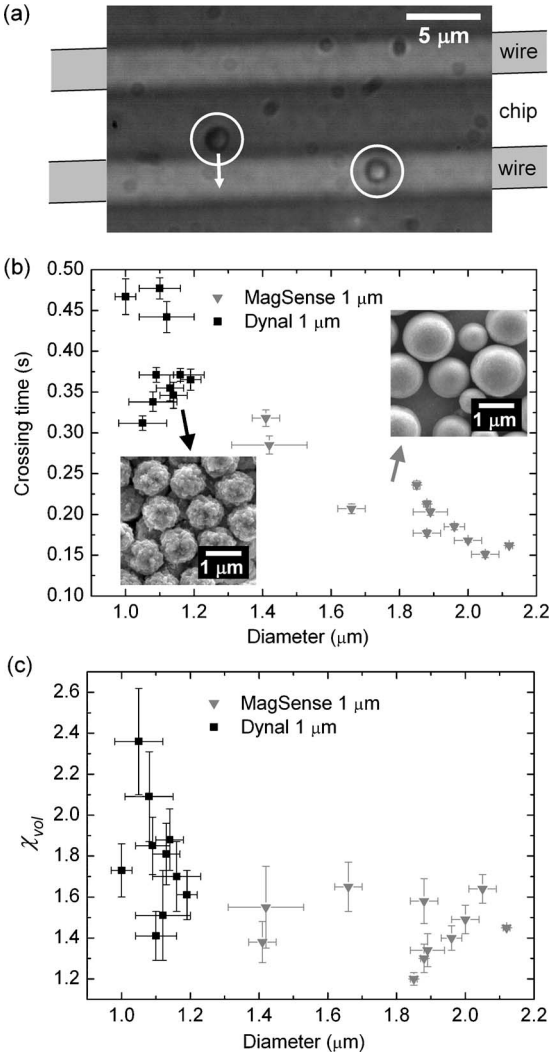

FIG. 1. (a) Microscope image of two Dynal particles, indicated by white circles, being pulled from top wire to bottom wire; other black spots in the picture are mainly dust on the camera lens. (b) Crossing time of individual particles between the wires (averaged over 15 transfers from upper to lower wire; current is 20 mA) as function of the optically determined diameter. Both Dynal 1 μm particles and MagSense 1 μm particles were measured. Also shown are SEM images of both particles. (c) Calculated volume susceptibility as function of the diameter.

rately after determining its size (for example, the average field gradient that a 2 μm particle experiences is a factor of 2.2 lower than the average field gradient that a 1 μm particle with equal χ_{par} experiences). The second parameter is the hydrodynamic drag coefficient f_d. Due to the proximity of the surface, the hydrodynamic drag is increased with a factor λ ($f_d^* = \lambda 6\pi\eta r$),[19,20]

$$\lambda = \left[1 - \frac{9}{16}\left(\frac{r}{h}\right) + \frac{1}{8}\left(\frac{r}{h}\right)^3 - \frac{45}{256}\left(\frac{r}{h}\right)^4 - \frac{1}{16}\left(\frac{r}{h}\right)^5\right]^{-1}, \tag{3}$$

where h is the distance from the particle center to the surface. This distance is mainly determined by the balance between the repulsive electrostatic force and the attractive magnetic force.[19] Using the approach of Leckband and Israelachvili[21] and rough estimations of the relevant parameters [ionic concentration of 500–750 μM by 1000× dilution of particle solution in de-ionized water, particle surface potential of −25 mV (measured), chip surface potential from −20 to −40 mV,[22] $\chi_{par}=2-3\times10^{-18}$ m^3, current of 20 mA, and distance particle-wire from 0 to 6 μm), we estimated that the particles move over the surface at a height between 40 and 130 nm. It should be noted that these estimations are not very accurate due to the large Debye length (10–15 nm) in our experiments, and common electrostatic interaction equations are only valid more than a few Debye lengths away. This height gives a correction factor λ between 2.5 and 1.9. Using $\lambda=2$ and $\eta=10^{-3}$ kg/m s, we estimated the particle and volume susceptibilities from the crossing times and plotted this in Fig. 1(c). For Dynal particles we found volume susceptibilities between 1.4 and 2.4; MagSense particles are slightly less magnetic, ranging from 1.2 to 1.7. In principle, these variations in volume susceptibility could be caused by differences in shape, resulting in a change in the demagnetization factor. However, inspection by SEM showed that both Dynal and MagSense particles are spherical. Consequently, the differences in susceptibility are attributed to their magnetic content. From vibrating sample magnetometer (VSM) measurement on bulk samples we measured the average volume susceptibility of Dynal particles to be 2.7, which is on the same order but slightly larger than the volume susceptibilities found in our experiments. The difference can be due to particle-particle interactions in the VSM measurements or due to a larger hydrodynamic drag than expected due to for example particle roughness.

It should be noted that we did not include a varying λ for particles with different susceptibilities and diameters in our experiments. Particles with a higher susceptibility could have a lower equilibrium height, leading to a higher λ and a lower χ_{vol} than in reality. We estimated that for particles of equal size an increase in susceptibility of a factor of two could lead to a 2%–3% change in λ, which is lower than our average measurement accuracy and can thus be neglected. Only in the extreme case of comparing a 1 μm particle with a 2 μm particle (equal χ_{vol}), the change in λ becomes noticeable (10%) but is still smaller than differences within particles. Therefore, on chip magnetophoretic analysis gives a good reflection of differences in particle properties.

B. High frequency fields

The application of magnetic fields by microscopic current wires rather than by external (electro)magnets gives the opportunity to study also the particle behavior at high frequencies. We measured eight particles in a magnetophoresis experiment where one wire was actuated with an ac current (square, switching between +V and −V) with frequencies in the range of 10–200 kHz. Figure 2 shows that the crossing time increased for increasing frequencies, up to 60% for a frequency of 200 kHz. This figure also shows that the difference between particles is quite large; at 50 kHz the increase in crossing time varies between 15% and 45%, and at 200 kHz the increase varies between 30% and 60%. Three out of eight particles seem to saturate after 50 kHz; five out of eight particles keep increasing their crossing time.

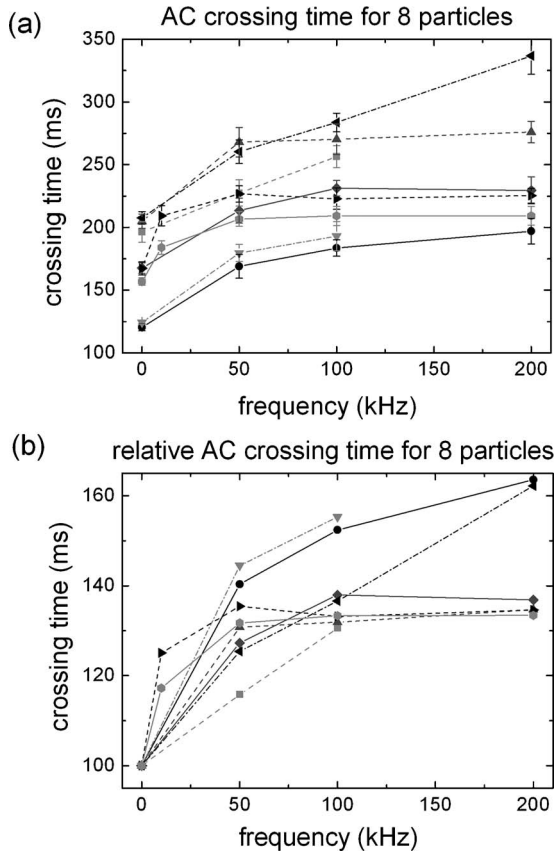

FIG. 2. (a) Crossing time of Dynal 1 μm particles as function of the field frequency. Each data point is the average of 9–13 crossings. (b) Change in crossing time relative to the dc value as function of the field frequency.

We can explain the increase in crossing time by considering the nonideally superparamagnetic grains of which the particles are composed, which have a certain distribution in size. In an ac field, part of the grains will follow the applied field, giving an unchanged contribution to the magnetic force, part of the grains follow but with a phase lag, giving a lower contribution, and part of the grains are not able to follow, giving no contribution. Thus, for increasing frequencies an increasing part of the grains stops to respond; therefore the high field susceptibility reduces. This effect has been measured before in bulk samples.[23] With on chip magnetophoresis information can be obtained from individual particles, and we indeed observed distinct differences between particles. The high field susceptibility and variations herein can, for example, be interesting for biosensor applications with giant magnetoresistance (GMR) or tunnel magnetoresistance (TMR) sensors, where high frequency modulation is used to increase the signal to noise ratio.[24,25]

It should be noted that the increase in crossing time can also be due to the existence of a permanent magnetic moment.[10] In a previous publication we measured in low-field rotation experiments a permanent magnetic moment in 3 μm particles up to 1% of the saturation magnetization, which can be about 30% of the induced low-field magnetization.[26] If this is also the case for 1 μm Dynal particles, they would have to physically rotate to align the permanent moment with the switching field. We calculated that this is not possible above frequencies of 500 Hz. The initial increase at the lowest measured frequency in Fig. 2 (10 or 50 kHz) can thus also be explained by a permanent magnetic moment; however, a permanent moment does not explain the additional increase for higher frequencies. More low-frequency measurements should be done to obtain information on the contribution of a permanent magnetic moment.

C. Wire channel setup

The experiments of the previous two sections showed that the accuracy of particle susceptibility determination is limited by two factors: the inhomogeneity of the field and the varying drag force on the particle due to close proximity of the chip surface. The field inhomogeneity leads to different average field gradients for differently sized particles, and the drag force varies for differently sized particles due to the close and nonfixed distance to the chip surface, which cannot be accurately determined by optical microscopy. This led us to consider an alternative chip design with larger wires on the chip surface, for example, wires with a cross-section of 10×15 μm^2, so the particle can move back and forth in the channel between the wires, as is shown in Fig. 3.

In the design of Fig. 3 particles are attracted to the center of the left wire when it is activated with a current. When the current in the left wire is turned off and the right wire is turned on, particles will move toward the right wire at a fixed and well-defined magnetic equilibrium height above the surface. We simulated this design and obtained field gradients above 0.5 T^2/m in fields lower than 10 mT. Interestingly, because the wire geometry is much larger, the field gradient is very uniform. The difference in average field gradient of a 1 μm particle and a 2 μm particle experience is only 1% (contrary to a factor of 2.2 in the previous design). Simulations showed that the confinement in the equilibrium height is plus or minus 0.5 μm, which gives only small variations in experienced field gradient (1%). The hydrodynamic drag on the particle will depend on the distance between particle and channel wall, but this can be corrected for when the particle position is measured by optical microscopy. There-

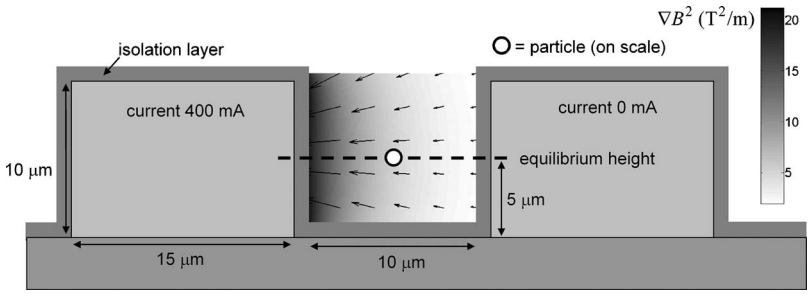

FIG. 3. Wire channel design for on chip magnetophoretic analysis. Magnetic particles are attracted to the center of the wire through which a current flows (left wire in the figure). When the left wire is turned off and the right wire is turned on, particles will cross the interwire channel at a fixed magnetic equilibrium height above the surface.

fore, we think that the wire channel design might be a further improvement for high accuracy magnetophoresis measurements.

In the previous sections we have shown chip designs suitable for dc and ac magnetophoretic analysis of 1 μm superparamagnetic particles. The accuracy of this technique is limited by Brownian motion [Eq. (2)]. This problem increases for decreasing particle size. For example, for 300 nm particles the field gradient should already be 25 times larger than for the 1 μm particles, which can be obtained by increasing the current five times, but that leads to considerable Joule heating and to fields above 10 mT. To overcome this problem, we have developed a technique that exploits the Brownian motion itself.[27] This technique will be described in the next section.

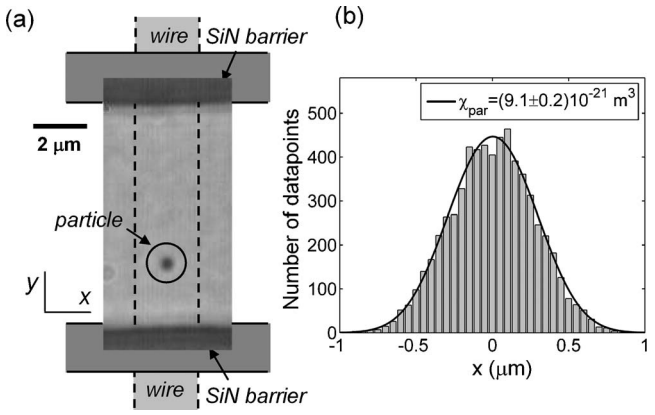

FIG. 4. (a) Ademtech 300 nm particle caught on current wire (vertical, depicted with dotted lines) between two SiN barriers (horizontal). (b) Histogram of the perpendicular (x) position of the particle measured at a current of 39 mA and the fitted theoretical distribution function.

IV. CONFINED BROWNIAN MOTION

In confined Brownian motion analysis, magnetic particles are caught in a magnetic potential well defined by a current wire on a chip.[27] The magnetic susceptibility is calculated from the thermal distribution of particle positions in the direction perpendicular to the wire,

$$P(x,y,z) \propto \exp\left(\frac{\chi_{\mathrm{par}}\mathbf{B}(x,y,z,I)^2/2\mu_o}{k_B T}\right). \quad (4)$$

χ_{par} is the particle susceptibility and $\mathbf{B}$ is the magnetic induction due to the current wire, which is dependent on the position (x,y,z) and the current I. The easiest way to apply this technique is in a two-dimensional potential well defined by a straight current wire, where the particle is still free to move parallel to the wire (y-direction). However, then one is limited by a short measurement time per particle; one particle can only be analyzed for about 10 s before either diffusing out of the field of view or before an increasing particle concentration on the wire leads to undesired particle-particle interactions.[27] In this section we will present two designs to catch individual particles in a three-dimensional potential well instead of a two-dimensional potential well, thus greatly enhancing the measurement time per particle. The capture in the third (y) dimension can be generated either sterically or magnetically.

A. Wire with surface barriers

One approach to capture individual particles in a three-dimensional potential well is using a chip with current wires where silicon nitride walls on the surface confine the particles to a certain part of the wire. The current wires (2.4 μm wide) were covered with a polished layer of 500 nm silicon nitride and an 80 nm gold layer that improves particle visibility and background uniformity to facilitate particle tracking. On the gold layer a pattern of silicon nitride walls (2 μm wide, between 500 nm and 1 μm high) was applied. The distance between the silicon nitride walls is 10 μm. When particles were captured on the current wires with typical currents of 30–50 mA, their freedom to move away from the surface was so low that they never crossed the walls. Using this technique, individual particles can be captured between two walls [Fig. 4(a)] and can be analyzed for at least 5 min.

Confined Brownian motion experiments were performed using Ademtech 300 nm particles. In Fig. 4(b) the resulting histogram of one particle is plotted. The histogram fits the theoretical distribution function well. In the theoretical distribution function the variations in particle size and the nonuniformity of the field are not taken into account because for 150–450 nm particles, this effect is small (at maximum a deviation of 5% between a 150 nm particle and a 450 nm particle, while their expected difference in susceptibility is an order of magnitude). The histograms of one particle for different currents return consistent susceptibility values.

We investigated the sources of errors in our measurements. Errors can, for example, occur due to limited statistics or due to the sensitivity of the measurement system (i.e., pixel resolution). We estimated the position sensitivity by repeatedly adding random noise of at maximum 1 pixel to the position data. We examined the role of limited statistics by dividing one measurement in intervals of increasing length. In Fig. 5 the error analysis results are shown, averaged for nine particles. The reproducibility error is (for optimal settings) always larger than the position sensitivity error. We can reach reproducibility errors below 10%. The behavior in this graph can be fitted well with $\sigma_{\mathrm{ave}} = \sqrt{\sigma_1^2/n + \sigma_2^2}$, with n the interval length (a purely statistical error would behave like $\sigma_{\mathrm{ave}} = \sigma_1/\sqrt{n}$). The found magnitude of σ_2 is 4.4%, which is larger than the determined sensitivity error of 2.7%. Therefore, apparently another error source is present, which we found to be mainly particle-surface interactions. The disturbance of particle-surface interactions in susceptibility measurements can be slightly reduced by changing experimental conditions such as the current or by varying surface properties by using for example a protein blocking agent such as bovine serum albumin or casein, but particle-surface interactions will probably always contribute to the error. Yet characterizing single-particle susceptibilities with errors below 10% is sufficient for the particle size range

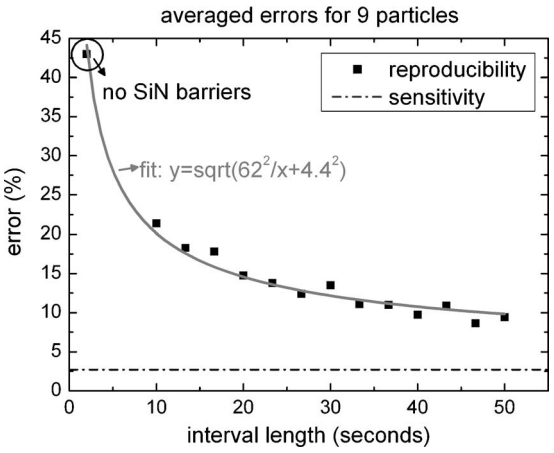

FIG. 5. Average reproducibility error as function of the interval length, averaged for nine particles. The reproducibility error is the standard deviation of the susceptibilities found when dividing the data in time intervals. The first point is the error without using surface barriers.[27] The error behavior is fitted with a square root relation. Also plotted (dash dotted line) is the error due to pixel sensitivity.

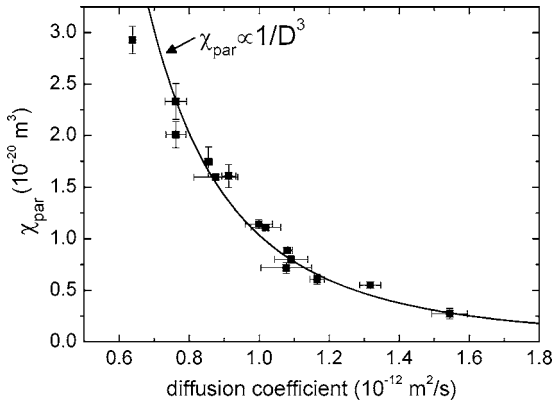

FIG. 6. Measured particle susceptibility χ_{par} of Ademtech 300 nm particles in confined Brownian motion experiments as function of the simultaneously measured diffusion coefficient. The data are fitted with $\chi_{par} \sim 1/D^3$.

of interest (100–1000 nm), where often variations in outer diameter up to a factor of three exist and variations in susceptibilities of an order of magnitude.

The Brownian motion technique can also be used to simultaneously obtain information on particle properties and particle kinetics. In the direction parallel to the wire the particle performs one-dimensional free diffusion from which the diffusion coefficient close to a surface can be calculated. The average distance a particle travels in a time t is given by $\langle x \rangle = 2\sqrt{Dt/\pi}$. By taking short timescales (33–167 ms) and position data more than 1 μm away from the barriers, we measured the diffusion coefficient for each particle (for longer timescales $\langle x \rangle$ stops being proportional to $\sqrt{t}$ due to the surface barriers). The absolute values of the diffusion coefficients that we found are $0.6-1.6\times10^{-12}$ m^2 s^{-1}. At an estimated temperature of 30 °C and viscosity of 0.82×10^{-3} kg/m s, the value of the diffusion coefficients of 150–450 nm particles should lie between 1.2 and 3.6 $\times10^{-12}$ m^2 s^{-1}. We can thus see a reduction due to the proximity of a surface of about 50%. Using Eq. (3) we can estimate the average distance of the nanoparticles above to surface to be about 30 nm.

The diffusion coefficient is inversely proportional to the radius, and the susceptibility is expected to be largely proportional to r^3; therefore we can expect $\chi_{par} \sim 1/D^3$. Figure 6 shows the susceptibility per particle as function of the diffusion coefficient, which can be fitted well using this relation. Thus, the susceptibility is indeed largely determined by the particle volume.

Finally, although the susceptibility measurements by confined Brownian motion analysis are disturbed by particle-surface interactions, the technique also offers the possibility to study these interactions. Contrary to common techniques to study particle-surface interactions, such as atomic force microscopy[28] or optical tweezers,[29,30] a particle trapped on a current wire is still free to move in one dimension (along the wire), and good statistical data can be obtained on favorite and less favorite positions. When trapping the larger Dynal 1 μm particles on a current wire (width of 3.4 μm, current of 20 mA) with a magnetic trapping force of around 4 pN (roughly four times larger than for the Ademtech particles in this section), we could clearly observe weak energy barriers ($\sim k_B T$) in the diffusion along the wire. We found that this interaction is a combination of particle and surface properties and nonspecific molecular interactions. Experiments with a series of well-controlled interactions (magnetic, electrostatic, and van der Waals) are needed to further characterize the Brownian motion technique for surface analysis.

B. Shaped wire

The other approach to capture the particle in three dimensions is by a magnetic field. This can be done with current wires that have narrow regions. In a narrow region the current density will be higher, thus attracting the particles. The shaped wires are 3.4 μm wide, and over a distance of 6.2–7.2 μm they narrow down to 2.4 μm [see Fig. 7(a)]. The resulting theoretical position distribution of the particle is plotted in Fig. 7(b) and shows that the wire effectively confines the particle to an ellipsoidal area above the narrowest part.

Our experiments show that individual Ademtech 300 nm particles can indeed be captured in the potential well and can be analyzed for at least 5 min. The histograms measured perpendicular to the wire direction and parallel to the wire direction are shown in Figs. 7(c) and 7(d). The resulting histograms have a reproducibility similar to that from the SiN barrier chips, so they give a good representation of the particle properties. However, the shape of the measured probability distribution is slightly different from the theoretical shape, resulting in a ratio of 1.6 between susceptibilities found in the parallel and perpendicular directions. For different particles this ratio varies slightly between about 1.5 and 2.

We consider three possible reasons for the difference in shape of the probability distribution: the magnetic field can be different than calculated, the fluid might move due to convection, or the particle magnetization can behave differently than expected. Simulations showed that the calculated field, and thus the shape of the potential well, is very sensitive to the dimensions of the wire. Using slight variations in

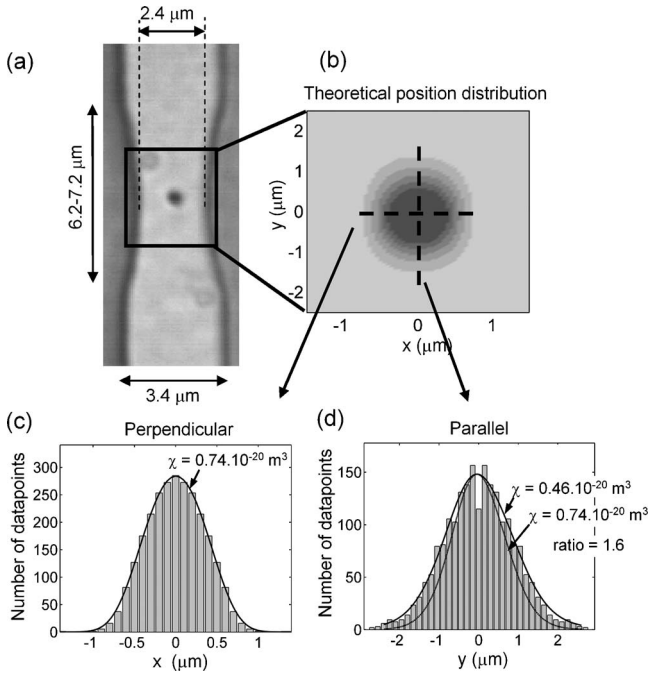

FIG. 7. (a) Ademtech 300 nm particle on a shaped wire. The wire dimensions have been measured in backscatter electron SEM images. (b) Theoretical position distribution calculated from the simulated current density in the wire. [(c) and (d)] Measured histograms of a particle on the *x*-*y* cross-sections through the center of the well, showing a ratio between found susceptibilities of 1.6. The dotted line in (d) shows the expected behavior with the measured susceptibility found in (c). The current was 42 mA.

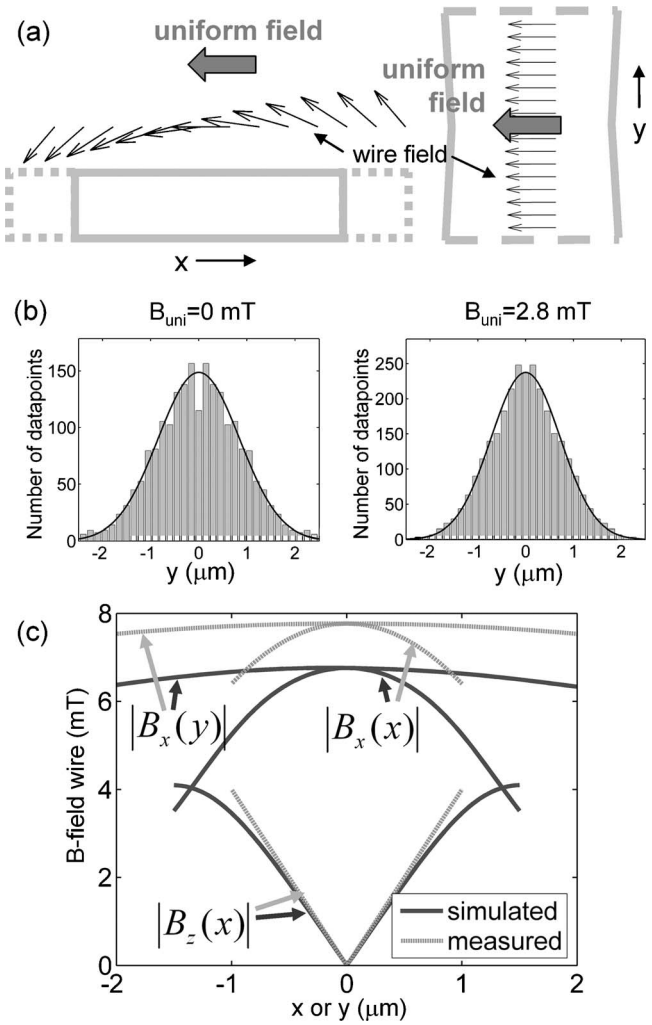

FIG. 8. (a) Field angle visualized above *x*- and *y* cross-sections of the shaped wire. The angle changes in the *x*-direction but is constant in the *y*-direction. (b) Two *y*-histograms of one Ademtech 300 nm particle measured at the same current (42 mA) through the wire with uniform fields of 0 and 2.8 mT. (c) Simulated and measured magnetic field profiles resulting from the combined fits of six data sets for one particle (three parallel and three perpendicular with uniform fields of 0, 1.4, and 2.8 mT).

wire dimensions, for example, 100 nm change in wire width, 200 nm change in simulation height, or 40 nm change in wire thickness, ratios between 1.1 and 2.0 can be obtained.

Next, a temperature gradient above the wire might lead to a convective fluid flow toward the center of the wire and upward, which can disturb the particle motion. We have measured the temperature rise in the wire to be at maximum 13 °C. Because the heat conductivity of water (0.6 W/m K) is not much lower than that of the silicon oxide chip surface (1.4 W/m K) and the thin silicon nitride cover layer (between 1.5 and 2.0 W/m K), we expect also a rise in water temperature. Due to the volume expansion of water at higher temperature, an upward buoyancy force is induced. However, because the temperature gradient is low and because the distance between the chip surface and the water-immersion lens is small (about 200 μm), the induced fluid speed is expected to be very low. Moreover, near the chip surface there is a no-slip condition, and due to symmetry the fluid velocity is zero at the center of the wire ($x=0$ μm). A numerical simulation showed a fluid velocity smaller than 0.01 μm/s within a few micrometers from the wire. This gives a maximum Stokes drag force on the particle of 0.03 fN, which is very small compared to the magnetic force (5–50 fN). Thus, we can neglect the influence of convection on the experiment.

Finally, it is possible that the particle properties influence the behavior in the potential well. In the direction perpendicular to the wire the field angle changes, and in the direction parallel to the wire the field angle is constant [see Fig. 8(a)]. If the magnetization in the particle does not follow the change in field angle instantly due to nonideal superparamagnetism or due to anisotropy, this will mainly cause a change in the perpendicular behavior. In contrast to the spherical shape of the 1 μm particles as discussed in the magnetophoretic analysis section, the Ademtech 300 nm particles show variations in shape. TEM images reveal that the particles are often nonspherical. A common shape is a flat cutoff on one side of the sphere, for example, an 80 nm thick slice cut off from a 400 nm particle. A simple simulation, taking the particle as built from independent elements and not considering demagnetization, shows that the difference in magnetic energy between upward and downward orientations of the cutoff part is about 1 k_BT. If then in the most extreme case due to, for example, demagnetization, the magnetization always stays in the horizontal direction ($\mathbf{B}^2$ only dependent on B_x^2), this causes a decrease in magnetic energy of up to 3.5 k_BT at the outer edges of the wire. These values can considerably influence the particle behavior in the potential well.

TABLE I. Found field parameters for five different particles in a shaped wire experiment using an external uniform field. The values of particle 2 are plotted in Fig. 8(c).

Particle	B_0 (mT)	B_{xdx}/B_{ydy}	$B_{zdx}{}^2/B_{xdx}$ [10^{-3} mT]
1	4.8 ± 3	17 ± 2	6.3 ± 0.2
2	7.7 ± 3	23 ± 6	12.0 ± 0.8
3	14.0 ± 5	21 ± 4	20.0 ± 0.6
4	3.8 ± 3	12 ± 2	2.5 ± 0.5
5	7.0 ± 3	6 ± 2	8.6 ± 0.4

We designed an experiment to examine the behavior of the particle magnetization. By adding an external uniform field in the x-direction (perpendicular to the wire and parallel to the chip surface), we can distinguish between the contributions of the $B_x(x)$ and $B_z(x)$ components in the total distribution. The reason is that in the parallel direction, the external uniform field influences the total magnetic energy but in the perpendicular direction only the fraction of the energy caused by the x-field parallel to the surface. We modeled the wire field components as $B_x(x,0)=B_0+B_{xdx}x^2$, $B_z(x,0)=B_{zdx}x$, and $B_x(0,y)=B_0+B_{xdy}y^2$, and substituted these components together with the uniform field $B_{\mathrm{uni},x}$ into Eq. (4) (see Appendix for explanation). By measuring the position distribution and fitting the model for at least two different $B_{\mathrm{uni},x}$, we can measure the four independent variables (B_0), (χB_{xdy}), (χB_{xdx}), and $(B_{zdx}{}^2/B_{xdx})$. These variables together give an estimation of the field that the particle experiences, and the resulting magnetization. For example, if the particle does not follow the field, which means it does not rotate its magnetization to the z-direction while moving away from the center in the x-direction, then the B_z-contribution will not show up in the distribution and therefore $(B_{zdx}{}^2/B_{xdx})$ will be zero.

Figure 8(b) shows two parallel histograms of one particle for external fields of 0 and 2.8 mT. The current through the wire is 42 mA. The external field is generated using a set of Helmholtz coils that fit around the microscope objective. The coils induce a homogeneous magnetic field, which is measured with a Gauss meter. From the combined fits of six data sets for one particle (three parallel and three perpendicular with uniform fields of 0, 1.4, and 2.8 mT), we calculated the magnetic field profile. The calculated profile is plotted together with the simulated field in Fig. 8(c). This figure shows that the maximum field is slightly higher, but the gradients are very similar to the simulated values. Because of the exponential factor in Eq. (4), a small change in field parameters can have a significant effect on the shape of the distribution function. The most interesting result is the matching value of the gradient in the B_z-field. Apparently, the particle is free to move its magnetization in the direction of the applied field and is not hindered much by anisotropy.

In Table I we listed the values found for six different particles. This table shows that there is quite a large variation in the found parameters. Although the parameters cannot be measured very accurately, they probably do indicate differences in particle properties such as anisotropy. The most striking is the fact that the found maximum field B_0 varies significantly, while it should be equal for all particles. An explanation for the variation in B_0 could be the existence of a permanent magnetic moment in the particles. A permanent moment would add an extra term $\mathbf{m}_{\mathbf{perm}}\cdot\mathbf{B}$ to the energy equation.[10] Assuming that the permanent moment is aligned to the field, this gives an addition to the B_0 factor, $B_0 \rightarrow B_0 + \mu_0 m_{\mathrm{perm}}/\chi$. This addition means that, for example, a 30% deviation in B_0 would point to a permanent magnetization of 30% of the induced magnetization. Since we use a low field (6.5 mT), this ratio might be possible. Thus, a permanent magnetic moment could explain the large value for particle 3 of Table I. However, particle 1 and particle 4 of Table I show a lower value than theoretical. This would mean that the permanent moment is aligned opposite to the field. We speculate that the induced magnetization might have another direction than the permanent magnetic moment due to particle anisotropy.

To give a definite answer on the size and orientation of permanent magnetization and anisotropy, it is necessary to measure the change in histogram width for different uniform fields with a better resolution. In our setup we were limited to a maximum uniform field of 3 mT, and as Fig. 8(b) shows, the change in width of the y-histogram is quite small. It would be advisable to use a uniform field of the order of the wire field (5–7 mT), which can be achieved using a different coil design. Furthermore, it is interesting to apply the shaped wire analysis to particles with a different ratio between the induced moment and the permanent moment, for example, particles composed (partly) of larger grains, leading to a possibly larger permanent moment, or ferromagnetic particles, where the induced moment might become almost negligible. Also, particles with a different shape anisotropy are worthwhile considering, for example, nonspherical particles. Thus, using a larger uniform field and using different particles, the possibility of studying multiple aspects of the magnetization of individual nanometer sized particles can be further investigated.

In the previous sections we have shown that confined Brownian motion analysis is a way to accurately measure the magnetic properties of submicrometer magnetic particles, which cannot be measured accurately using magnetophoretic analysis. We showed two variations in confined Brownian motion analysis to capture the particles on the chip surface in three dimensions, namely, using either surface barriers to confine the particles to a certain part of the wire or using shaped wires to confine the particles magnetically in all dimensions.

V. CONCLUSIONS

We have shown several chip designs that constitute a toolbox for the characterization of particle properties and dynamics. We demonstrated a chip design suitable for magnetophoretic analysis of 1 μm superparamagnetic particles. We measured the crossing time between two current wires for two types of particles, Dynal 1 μm and MagSense 1 μm particles, with an accuracy of 3%–5%. From the crossing times we calculated the volume susceptibilities. Although Dynal particles are very uniform in outer diameter, their vol-

ume susceptibilities still varied between 1.4 and 2.4. MagSense particles were more polydisperse in outer diameter and slightly less magnetic than Dynal particles with volume susceptibilities between 1.2 and 1.7. The magnetophoresis chip is also suitable for measuring the high frequency susceptibility. Due to the grain size distribution in superparamagnetic particles, we expected a decrease in high frequency susceptibility. Crossing time measurements using ac currents from 10–200 kHz indeed showed an increase in crossing time up to 60% with distinctly different behavior between particles. Finally, we suggested an alternative chip design using larger wires, where particles can move back and forth in the channel between the wires. This design might be a further improvement for high accuracy magnetophoresis measurements.

Submicrometer particles were characterized using two chip designs for Brownian motion analysis of captured particles on a current wire. In one design we used surface barriers to confine particles to a certain area of the wire, thus improving the measurement time per particle. For 300 nm particles this technique led to measurements of the susceptibility with an accuracy better than 10%. Simultaneously with the susceptibility also the diffusion coefficient of the particle was determined. We found a reduction of 50% in diffusion coefficient compared to the expected bulk values due to close proximity of the chip surface. In the other design we captured the particles magnetically in three dimensions using a current wire with narrow regions. This also led to accurate particle characterization but showed a deviation from theory in the three-dimensional position distribution. The deviation was most probably due to slightly different wire dimensions but could also partly be due to particle anisotropy. Using an additional uniform field we could give an estimation of the particle magnetization induced by the applied field, and we saw that anisotropy does not prevent a particle from rotating its magnetization in the direction of the applied field.

This paper demonstrates that monitoring the dynamics of individual micro- and nanoparticles near a chip surface is a promising tool to accurately quantify magnetic properties such as susceptibility, ac susceptibility, permanent magnetization, and anisotropy. We expect that with this knowledge particle detection, transport, and manipulation in magnetic particle-based biosensors and lab-on-a-chip applications can be improved.

APPENDIX: UNIFORM FIELD IN SHAPED WIRE ANALYSIS

Using an additional external uniform field in confined Brownian motion analysis, Eq. (4) becomes

$$\ln[P(x,y)] = \ln(C) + \frac{\chi_{\text{bead}}}{2\mu_0 k_B T} \cdot (B_x{}^2 + 2B_x B_{\text{uni},x} + B_z{}^2 + B_{\text{uni},x}{}^2).$$

$B_{\text{uni},x}$ is the uniform field applied in the x-direction. B_x and B_z are the components of the wire field in x-direction and z-direction. We do not consider B_y because B_y is more than an order of magnitude smaller than B_x and B_z in the region of interest and therefore is negligible. C is the normalization constant. Next, we consider only the two position distribution histograms at the $x=0$ and $y=0$ cross-sections, and we model the field as $B_x(x,0)=B_0+B_{xdx}x^2$, $B_z(x,0)=B_{zdx}x$, and $B_x(0,y)=B_0+B_{xdy}y^2$. These equations show that at the center of the well, the B_x-field has a maximum value, and moving away from the center in either direction $(+x,-x,+y,-y)$, the field will decrease in first order approximation with an x^2-dependence for small distances. From symmetry considerations, it follows that at the center of the well, the B_z-field is zero. Therefore $B_z(0,y)=0$ and $B_z(x,0)$ will become positive in one direction and negative in the other direction; thus in first approximation this can be modeled by an x-dependence.

The fitting functions for the two histograms then become

$$\ln[P(x)] = C_0 + \chi/(2\mu_0 k_B T)(2B_0 B_{xdx} + 2B_{\text{uni},x}B_{xdx} + B_{zdx}{}^2)x^2 + O(x^4),$$

$$\ln[P(y)] = C_0 + \chi/(2\mu_0 k_B T)(2B_0 B_{xdy} + 2B_{\text{uni},x}B_{xdy})y^2 + O(y^4).$$

In both equations C_0 represents a series of constants, among which is the normalization constant. These constants are not important for further calculations. The last fourth order term can be neglected because this is much smaller than the second order term. The equation for the y-direction has three unknowns: the susceptibility χ, the maximum field B_0, and the field gradient B_{xdy}. By measuring the x- and y-distributions for two different $B_{\text{uni},x}$, the two variables B_0 and χB_{xdy} can be solved. Using B_0 and the x-equation then gives the variables χB_{xdx} and $B_{zdx}{}^2/B_{xdx}$. The four variables together give an estimation of the field the particle experiences and the resulting magnetization.

[1] Q. A. Pankhurst, J. Conolly, S. K. Jones, and J. Dobson, J. Phys. D **36**, R167 (2003).
[2] A. M. Gijs, Microfluid. Nanofluid. **1**, 22 (2004).
[3] N. Pamme, Lab Chip **6**, 24 (2006).
[4] R. J. S. Derks, A. J. H. Frijns, M. W. J. Prins, and A. H. Dietzel, Appl. Phys. Lett. **92**, 024104 (2008).
[5] D. L. Graham, H. A. Ferreira, and P. P. Freitas, Trends Biotechnol. **22**, 455 (2004).
[6] M. W. J. Prins and M. Megens, *Encyclopedia of Materials: Science and Technology* (Elsevier, Amsterdam, 2007), pp. 1–6.
[7] X. J. A. Janssen, L. J. van IJzendoorn, and M. W. J. Prins, Biosens. Bioelectron. **23**, 833 (2008).
[8] B. G. Hosu, K. Jakab, P. Bánki, F. I. Tóth, and G. Forgacs, Rev. Sci. Instrum. **74**, 4158 (2003).
[9] M. Panhorst, P. Kamp, G. Reiss, and H. Brückl, Biosens. Bioelectron. **20**, 1685 (2005).
[10] S. S. Shevkoplyas, A. C. Siegel, R. M. Westervelt, M. G. Prentiss, and G. M. Whitesides, Lab Chip **7**, 1294 (2007).
[11] A. C. Siegel, S. S. Shevkoplyas, D. B. Weibel, D. A. Bruzewicz, A. W. Martinez, and G. M. Whitesides, Angew. Chem. **118**, 7031 (2006); Angew. Chem., Int. Ed. **45**, 6877 (2006).
[12] J. C. Crocker and D. G. Grier, J. Colloid Interface Sci. **179**, 298 (1996).
[13] S. J. Gill, C. P. Malone, and M. Downing, Rev. Sci. Instrum. **31**, 1299 (1960).
[14] S. Reddy, L. R. Moore, L. Sun, M. Zborowski, and J. J. Chalmers, Chem. Eng. Sci. **51**, 947 (1996).
[15] H. Watarai, M. Suwa, and Y. Iiguni, Anal. Bioanal. Chem. **378**, 1693 (2004).
[16] U. O. Häfeli, M. A. Lobedann, J. Steingroewer, L. R. Moore, and J. Riffle, J. Magn. Magn. Mater. **293**, 224 (2005).
[17] S. Chikazumi, *Physics of Magnetism* (Wiley, New York, 1964).

[18]C. D. Meinhart, S. T. Werely, and J. G. Santiago, Exp. Fluids **27**, 414 (1999).
[19]R. Wirix-Speetjens, W. Fyen, K. Xu, J. De Boeck, and G. Borghs, IEEE Trans. Magn. **41**, 4128 (2005).
[20]J. Happel and H. Brenner, *Low Reynolds Number Hydrodynamics* (Kluwer, Dordrecht, 1991).
[21]D. Leckband and J. Israelachvili, Q. Rev. Biophys. **34**, 105 (2001).
[22]I. Sokolov, Q. K. Ong, H. Shodiev, N. Chechik, D. James, and M. Oliver, J. Colloid Interface Sci. **300**, 475 (2006).
[23]P. C. Fannin, L. Cohen-Tannoudji, E. Bertrand, A. T. Giannitsis, C. Mac Oireachtaigh, and J. Bibette, J. Magn. Magn. Mater. **303**, 147 (2006).
[24]B. M. de Boer, J. A. H. M. Kahlman, T. P. G. H. Jansen, H. Duric, and J. Veen, Biosens. Bioelectron. **22**, 2366 (2007).
[25]M. Megens, F. de Theije, B. de Boer, and F. van Gaal, J. Appl. Phys. **102**, 014507 (2007).
[26]X. J. A. Janssen, A. J. Schellekens, K. van Ommering, L. J. van IJzendoorn, and M. W. J. Prins, Biosens. Bioelectron. **24**, 1937 (2009).
[27]K. van Ommering, J. H. Nieuwenhuis, L. J. van IJzendoorn, B. Koopmans, and M. W. J. Prins, Appl. Phys. Lett. **89**, 142511 (2006).
[28]B. Gady, D. Schleef, R. Reifenberger, D. Rimai, and L. P. DeMejo, Phys. Rev. B **53**, 8065 (1996).
[29]P. M. Hansen, J. K. Dreyer, J. Ferkinghoff-Borg, and L. Oddershede, J. Colloid Interface Sci. **287**, 561 (2005).
[30]D. C. Prieve, Adv. Colloid Interface Sci. **82**, 93 (1999).